On gravity-driven flow through a reacting porous rock

By ALAN W. V. RAW[1,2] and ANDREW W. WOODS[1]

[1]BP Institute for Multiphase Flow, University of Cambridge, Cambridge CB3 0EZ, UK

[2]Mathematics Department, University of Bristol, Bristol BS8 1TW, UK

We develop a model to describe the spreading of a reacting liquid which is injected at a steady rate into a permeable rock. We focus on the case in which there is a density difference between the host reservoir fluid and the injected liquid. We examine reactions which lead to precipitation and a decrease in permeability or dissolution and an increase in permeability. In both cases, we assume the reaction is rapid compared to the speed of the flow. As the current spreads under gravity, we show that the interface between the injected fluid and the original fluid and also the reaction front, may be described by similarity solutions. The morphology of the two interfaces is controlled by two parameters: the permeability ratio across the reaction front, k, and the speed of the reaction front as a fraction of the interstitial speed, λ. For a precipitation reaction, the reaction front lags some distance behind the leading edge of the region occupied by the injected fluid, and tends to terminate in a sharp vertical front. In contrast, for a dissolution reaction, the reaction front migrates as a gravity-driven finger along the base of the formation. In the case of large changes in permeability, $k\lambda > 1$, this finger advances to the front of the flow, whereas for smaller increases in permeability, $k\lambda < 1$, the finger is overrun with injected fluid which has already reacted and passed through the reaction front. We illustrate how these results are affected if the density of the reacting fluid decreases across the reaction zone. In the case of precipitation, small changes in density smooth out the leading edge of the reaction front, whereas large changes in density lead to slumping of the reaction front along the base of the current, and ultimately it extends to the nose of the flow. For dissolution reactions, the decrease in density across the reaction front causes the lateral extent of the finger to increase. As a result the critical value of the permeability ratio, k, for which the reaction front reaches the nose of the current decreases.

1. Introduction

There are numerous different types of reactions which may arise in porous rocks (Phillips 1991). These include frontal reactions, which advance through the formation with the injected fluid; gradient reactions, which arise when the fluid moves through a temperature gradient in the formation because of the temperature dependence of the solubility of the minerals in solution; and mixing reactions, which arise when two fluids of different composition mix in the formation. In this paper, we focus on frontal reactions which are typically associated with the injection of fluid of one composition into a porous formation initially saturated with fluid of a second composition (Chadam *et al.* 1986; Ortoleva *et al.* 1987; Hinch & Bhatt 1990; Ormond

& Ortoleva 2000). Such reactions can have an important impact on the flow as they change the properties of the rock, and in particular, the permeability.

Precipitation of minerals in the pore spaces decreases the permeability. Such fronts tend to be dynamically stable in the sense that the permeability increases and therefore the pressure gradient decreases in the direction of flow. In contrast, a dissolution front leads to formation of higher permeability rock near the source of the injected fluid. In turn, this leads to an adverse pressure gradient across the reacting front, with the permeability decreasing in the direction of flow. As a consequence, the dissolution front may become unstable to a fingering instability which leads to the formation of preferential flow channels (Ortoleva *et al.* 1987; Hinch & Bhatt 1990; Keleman *et al.* 1995). These flow channels result in the injected fluid bypassing much of the original formation, and tend to produce reaction veins within the original formation (Ortoleva *et al.* 1987; Phillips 1991).

Although the flow and stability of such reaction fronts have been studied for purely pressure driven flow, in many systems, the density of the injected fluid will be different from the host fluid, owing to the different chemical composition of the fluids. In such a regime, the buoyancy forces associated with the difference in density between the two fluids, rather than an externally imposed pressure, may control the flow. The purpose of this paper is to examine the morphology and rate of spreading of the reaction front in such a gravity driven flow. Following the predictions of models of gravity currents in porous rocks (Huppert & Woods 1995; Woods & Mason 2000), we might expect that the dense injected liquid will spread along the lower boundary of the reservoir leading to a different morphology of the reaction front which trails behind.

In §2, we develop a model to describe the evolution of the injected liquid and of the reacting interface with time. In §3, we develop a series of similarity solutions for this flow in the case where the density difference between the injected liquid and the host fluid remains approximately constant across the reaction front. These solutions identify the important differences between precipitation and dissolution reactions. In §4, we generalize the analysis to allow for changes in density of the injected fluid across the reaction front. In §5, we discuss the relevance of the modelling both for industry and in natural flow regimes, and draw some conclusions in §6.

2. The model

2.1. *Reaction dynamics*

Numerous workers have studied the structure of reaction fronts associated with a uniform flow through a porous rock (Ortoleva *et al.* 1987; Hinch & Bhatt 1990; Phillips 1991). In the reaction zone, the concentration of reactant (moles per unit volume) in the liquid falls from the upstream source concentration c_o to zero, while the concentration of mineral in the matrix (moles per unit volume) increases from zero, upstream of the reaction zone, to the unreacted value s_o downstream (figure 1). The reaction may be characterized by a kinetic rate constant, τ say, and a reaction law that for a given reaction, υ moles of reactant A in the solid react with one mole of reactant B in the fluid. If the fluid migrates through a porous rock with Darcy speed u, then any reaction zone associated with the flow will extend a distance of order $u\tau/\phi$. For times t long compared to τ, the reaction front is localized compared to the zone which is occupied by the injected fluid (e.g. Phillips 1991; Hinch & Bhatt 1990). For a localized reaction front, the ratio of the speed of the reaction front
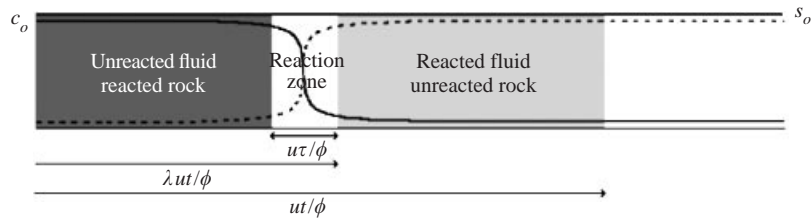
FIGURE 1. Illustration of a reaction zone showing the liquid reactant supplied upstream of the front and the distribution of reactant on the rock as a function of position across the reaction front. Concentration of reactant ——, in the liquid and - - - -, in the rock matrix.

to the interstitial speed of the fluid, λ say, may be found by using a simple mass balance. If a steady, one-dimensional flow, with Darcy speed u, advances into a rock of porosity ϕ, then after time t, the region invaded with liquid extends a distance ut/ϕ ahead of the source, while the reaction front is located a distance $\lambda ut/\phi$ ahead of the source (figure 1). Therefore, a volume of rock $\lambda(1 - \phi)ut/\phi$, which contains $\lambda(1 - \phi)uts_o/\phi$ moles of reactant A, has reacted with a volume $\phi(1 - \lambda)ut/\phi$ of fluid containing $\phi(1 - \lambda)utc_o/\phi$ moles of reactant B. Since the reaction requires v moles of solid reactant A per mole of fluid reactant B we deduce that

$$\lambda = \frac{\phi c_o}{v(1 - \phi)s_o + \phi c_o}.$$ (1)

The reaction may lead to an increase or a decrease in the porosity and permeability of the rock. The relation between porosity and permeability is complex and depends in detail on the structure of the porous matrix. Typically, small changes in porosity may lead to much larger changes in permeability, especially if the permeability is controlled by narrow throats which connect pore spaces. For example, the porosity–permeability relation in fractured rock is quite different from that in a porous sandstone or other sedimentary deposit (Dullien 1992). For simplicity, we assume that the change in porosity across the reaction zone is so small that we can take it to be a constant, while the permeability changes from value k_1 downstream to value k_2 upstream of the reaction front. This approximation is likely to be most applicable to situations in which the reaction causes small changes to the precipitate deposit in the pore throats, since these may provide the main resistance to the flow, yet contribute only a small part of the porosity (Dullien 1992). ρ denotes the density of the fluid originally in place in the reservoir. We denote the density of the injected fluid as $\rho + \Delta\rho_u$ and $\rho + \Delta\rho_l$ downstream and upstream of the reaction front. In this work, we focus on the case that $0 > \Delta\rho_l > \Delta\rho_u$ so that the density of the reacted fluid is intermediate between that of the relatively dense injected fluid and the relatively buoyant formation fluid, leading to the flow configuration shown in figure 2.

2.2. *Flow dynamics*

We now consider the motion of dense injected fluid which spreads along the base of the reservoir. We model a one-dimensional flow as appropriate for injection of fluid from a horizontal well, which acts as a line source. The modelling approach may be readily extended to include axisymmetric flows from a point source, but this is beyond the scope of the present study. After some time, the fluid will form a thin, laterally extensive current (figure 2) in which the vertical pressure is approximately hydrostatic (Huppert & Woods 1995). We denote the upper surface of the injected fluid as $h_u(x,t)$ and the upper surface of the reaction front, which lags behind the
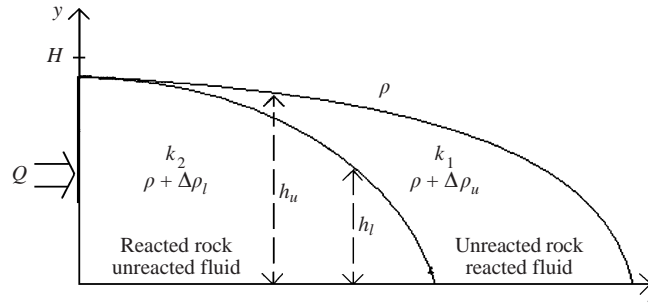
FIGURE 2. Schematic illustrating the motion of a gravity driven reaction front and the injected dense liquid.

injected fluid, as $h_l(x,t)$ (figure 2). If y denotes the elevation of a point above the lower boundary, then the pressure at the point (x,y) has value

$$p = p_o + \rho g(H - y) + \Delta \rho_l g(h_l - y) + \Delta \rho_u g(h_u - h_l) \quad \text{for} \quad 0 < y < h_l, \qquad (2)$$

corresponding to the region of reacted rock flooded with unreacted injected liquid and has value

$$p = p_o + \rho g(H - y) + \Delta \rho_u g(h_u - y) \quad \text{for} \quad h_l < y < h_u, \qquad (3)$$

corresponding to the region of unreacted rock flooded with the reacted injected liquid. Here, p_o is the reference pressure at height H above the boundary. The speed of the flow in the region $h_u > y > h_l$, which is filled with injected but reacted fluid, which has passed through the reaction zone is given by Darcy's law

$$u_u = -\frac{k_1 g \Delta \rho_l}{\mu} \frac{\partial h_u}{\partial x}, \qquad (4)$$

while the speed of the injected but unreacted fluid advancing towards the reaction zone is

$$u_l = -\frac{k_2 g}{\mu} \left[(\Delta \rho_l - \Delta \rho_u) \frac{\partial h_l}{\partial x} + \Delta \rho_u \frac{\partial h_u}{\partial x} \right]. \qquad (5)$$

The rate of ascent of the reaction front, $\partial h_l / \partial t$ is given from the conservation of mass noting that the reaction front migrates at a fraction λ/ϕ of the vertical transport velocity (equation (1)),

$$\phi \frac{\partial h_l}{\partial t} = -\lambda \frac{\partial h_l u_l}{\partial x}. \qquad (6)$$

The remainder of this vertical flux, $(1 - \lambda)/(\partial h_l u_l / \partial x)\phi$ passes through the reaction front into the upper layer of injected fluid where it causes the upper layer to deepen according to the relation

$$\phi \frac{\partial (h_u - h_l)}{\partial t} = -(1 - \lambda) \frac{\partial h_l u_l}{\partial x} - \frac{\partial (h_u - h_l) u_u}{\partial x}. \qquad (7)$$

Here, the last term on the right-hand side corresponds to the divergence of the fluid flux in the upper layer, which can also change the depth of the upper layer. By combining the expressions for u_l and u_u in terms of h_l and h_u with equations (6) and (7) we are able to derive two nonlinear equations for the evolution of the reaction front and the leading edge of the injected fluid in this gravity driven flow. To simplify the algebra, it is useful to introduce two dimensionless variables. The buoyancy ratio

is defined as

$$R = \Delta\rho_l/\Delta\rho_u, \tag{8}$$

and the permeability ratio

$$k = k_2/k_1. \tag{9}$$

We also introduce a dimensional scale for the velocity

$$S = k_1\Delta\rho_u g/\phi\mu. \tag{10}$$

This leads to the governing equations

$$\frac{\partial h_l}{\partial t} = Sk\lambda\frac{\partial}{\partial x}\left(h_l\frac{\partial h_u}{\partial x} + (R-1)h_l\frac{\partial h_l}{\partial x}\right), \tag{11}$$

and

$$\frac{\partial h_u}{\partial t} = S\frac{\partial}{\partial x}\left[((k-1)h_l + h_u)\frac{\partial h_u}{\partial x} + k(R-1)h_l\frac{\partial h_u}{\partial x}\right]. \tag{12}$$

It may be seen from equations (11) and (12) that the three controlling parameters are the permeability ratio across the reaction front, k, the buoyancy ratio, R, and the reaction parameter λ. Since there are three controlling parameters, the range of flow behaviour is varied and it is instructive, in the first instance, to consider cases in which $R = 1$ so that the fluid buoyancy does not change as a result of the reaction. This may occur if saline fluid, carrying a low concentration of reactant which has a negligible effect on the density, displaces relatively fresh host water in the porous layer. This situation may arise, for example, during a replacement reaction, such as the dolomitization of limestone, when magnesium rich sea-water displaces relatively fresh water from the formation (Phillips 1991).

3. Flows with no density change across the reaction, $R = 1$

In this situation, the governing equations reduce to the simpler form

$$\phi\frac{\partial h_l}{\partial t} = Sk\lambda\frac{\partial}{\partial x}\left(h_l\frac{\partial h_u}{\partial x}\right), \tag{13}$$

and

$$\phi\frac{\partial h_u}{\partial t} = S\frac{\partial}{\partial x}\left([h_u + (k-1)h_l]\frac{\partial h_u}{\partial x}\right). \tag{14}$$

Since these equations are coupled nonlinear diffusion-type equations, then for a constant injection rate, we expect shape-preserving self-similar solutions. For a steady injection rate Q per unit length, we seek solutions of the form

$$h_l = \gamma(\omega t)^{1/3}f_l(\eta), \quad h_u = \gamma(\omega t)^{1/3}f_u(\eta), \tag{15}$$

where $\eta = x/\gamma(\omega t)^{2/3}$, $\gamma = Q/S$ and $\omega = S^2/Q$. Note that γ has units of length and ω has units $1/$time. Now the shape functions f_l and f_u satisfy the relations

$$f_l - 2\eta\frac{\mathrm{d}f_l}{\mathrm{d}\eta} = 3\lambda k\frac{\mathrm{d}}{\mathrm{d}\eta}\left(f_l\frac{\mathrm{d}f_u}{\mathrm{d}\eta}\right), \tag{16}$$

and

$$f_u - 2\eta \frac{df_u}{d\eta} = 3\frac{d}{d\eta}\left((f_u + (k-1)f_l)\frac{df_u}{d\eta}\right). \tag{17}$$

The shape functions f_l and f_u represent the shape of the reaction front and of the leading edge of the injected liquid which drives the reaction. The form of the solution depends critically on the two parameters k and λ. We have solved the nonlinear coupled equations (16) and (17) numerically to find the shape functions f_u and f_l.

3.1. *Boundary conditions*

In solving the equations, we require a number of boundary conditions. First, at the source, all the fluid flux consists of unreacted fluid. This requires that

$$(f_l - f_u)\frac{df_u}{d\eta} = 0 \quad \text{at} \quad \eta = 0. \tag{18}$$

In order that there is a net flux, this requires that $f_l = f_u$ at $\eta = 0$. Secondly, at the source, the flux of unreacted fluid is a constant, so that

$$-\phi k f_l \frac{df_u}{d\eta} = 1 \quad \text{at} \quad \eta = 0. \tag{19}$$

This provides a relation between $f_l(0)$ and $(df_u/d\eta)(0)$. From equations (16) and (17), we may then determine $df_u/d\eta$ and $d^2f_u/d\eta^2$ in terms of f_l at $\eta = 0$. Finally, the solutions should satisfy the conservation of fluid

$$\int_o^{\eta_e} f_u\,d\eta = \frac{1}{\phi}, \tag{20}$$

and the conservation of reactant, as expressed by the relation

$$\int_o^{\eta_e} f_l\,d\eta = \frac{\lambda}{\phi}. \tag{21}$$

Depending on the conditions, the reaction zone may or may not extend the full length of the current, $\eta = \eta_e$.

In the case where the reaction zone does not reach the end of the current, the flow of reacted liquid through the unreacted rock ahead of the reaction zone is governed by the relation

$$f_u - 2\eta \frac{df_u}{d\eta} = 3\frac{d}{d\eta}\left(f_u \frac{df_u}{d\eta}\right). \tag{22}$$

At the point where the reaction zone ends, $\eta = \eta_r$, the depth of the upper interface, f_u, varies continuously and the total mass flux is continuous

$$f_u \frac{df_u}{d\eta}\bigg|_{\eta_r+} = (f_u + (k-1)f_l)\frac{df_u}{d\eta}\bigg|_{\eta_r-}. \tag{23}$$

On solving the equations, three types of solution emerge, and we describe these below. We note here, however, that although equations (16) and (17) are second order in f_u, they are only first order in f_l and so may admit solutions which are discontinuous in f_l while being continuous in f_u. Indeed, we find that, when $k < 1$, a shock forms at the leading edge of the reaction front where f_l suddenly decreases to zero. In contrast, when $k > 1$, the dissolution zone at the base of the current extends smoothly to zero depth.
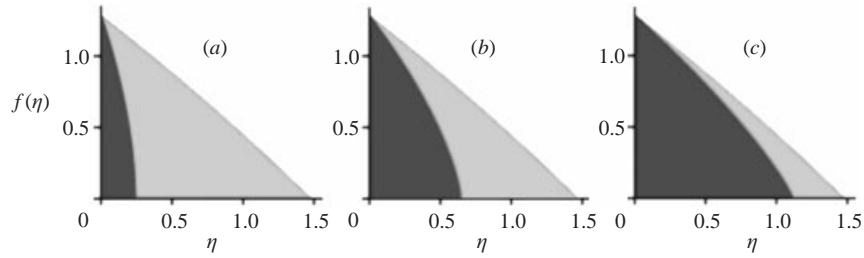
FIGURE 3. Calculations showing the shape of the reaction front and the distribution of the injected liquid in the case where there is no change in permeability due to the reaction. Calculations are shown for permeability ratio $k = 1$ with (a) $\lambda = 0.2$, (b) 0.5, (c) 0.7.

3.2. Constant permeability solutions, $k = 1$

If there is no change in the permeability associated with the reaction, $k = 1$, then the structure of the solution depends only on the value of λ (figure 3). For small λ, a large quantity of liquid is required to react with unit mass of rock, and hence a large intrusion of reacted fluid develops ahead of the reaction front (figure 3a). For larger values of λ, less liquid is required per unit mass of reacted rock, and so the reaction zone largely overlaps with the region occupied by injected fluid (figure 3c).

3.3. Dissolution solutions, $k > 1$

If the reaction leads to dissolution of the rock, then the injected fluid tends to run rapidly through the high-permeability reacted zone along the base of the layer before moving across the reaction front and into the low-permeability host rock (figure 4). This leads to the formation of a narrow high-permeability channel along the lower boundary of the reservoir. As fluid passes through this reaction front into the lower permeability host rock, the flow decelerates, and the fluid tends to accumulate above the reaction front. If the speed of the reaction front is similar to the interstitial flow speed ($\lambda \sim 1$) or there is a large increase in permeability as a result of the reaction, $k \gg 1$, then the reaction zone extends to the nose of the current (figure 4b–d). We describe this as a *strong dissolution reaction*. However, if a very large mass of liquid is required to react with unit mass of rock ($\lambda \ll 1$) or there is a very small change in permeability, then the reacted fluid is able to run far ahead of the reaction front (figure 4a). We call this a *weak dissolution reaction*. A numerical parameter study (figure 5) has identified that the transition from one regime to the other occurs when $k\lambda = 1$. The origin of this criterion may be seen by considering the asymptotic behaviour of the current near the nose. From equations (16) and (17), we find that if both layers extend to the nose of the flow, then near the nose,

$$f_u \sim \frac{2\eta_e}{3\lambda k}(\eta_e - \eta) \quad \text{for} \quad \eta < \eta_e, \quad (\eta_e - \eta) \ll \eta_e, \tag{24}$$

$$f_l \sim \left(\frac{k\lambda - 1}{k - 1}\right) \frac{2\eta_e}{3\lambda k}(\eta_e - \eta) \quad \text{for} \quad \eta < \eta_e, \quad (\eta_e - \eta) \ll \eta_e. \tag{25}$$

In order that both $f_l > 0$ and $f_u > 0$, we require that $k\lambda > 1$. In the limiting condition $k\lambda = 1$, the depth of the reaction zone just falls to zero at the nose, whereas for smaller values of $k\lambda$, the leading edge of the reaction zone lags behind the nose of the current.
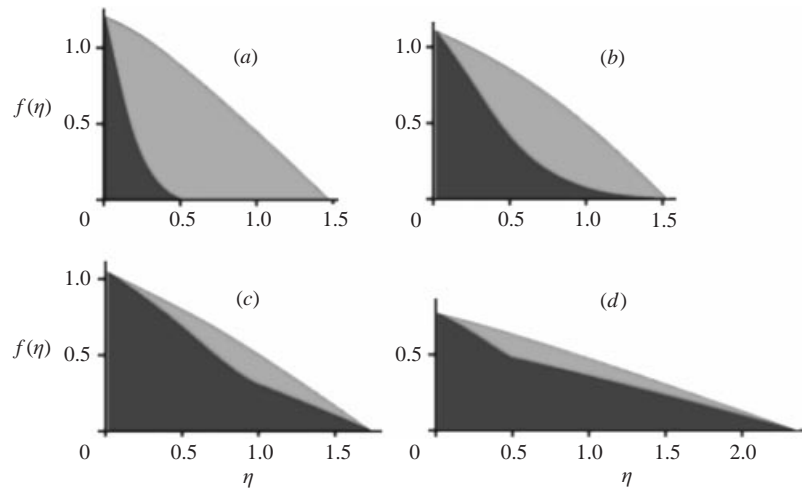
FIGURE 4. Calculations showing the shape of the reaction front and the distribution of the injected liquid in the case of a dissolution reaction. Calculations are shown for permeability ratios $k = 2$ with (a) $\lambda = 0.2$, (b) 0.5, (c) 0.8, and for (d) $k = 5$ with $\lambda = 0.8$. Cases (a) and (b) correspond to weak dissolution reactions, whereas cases (c) and (d) correspond to strong dissolution reactions.
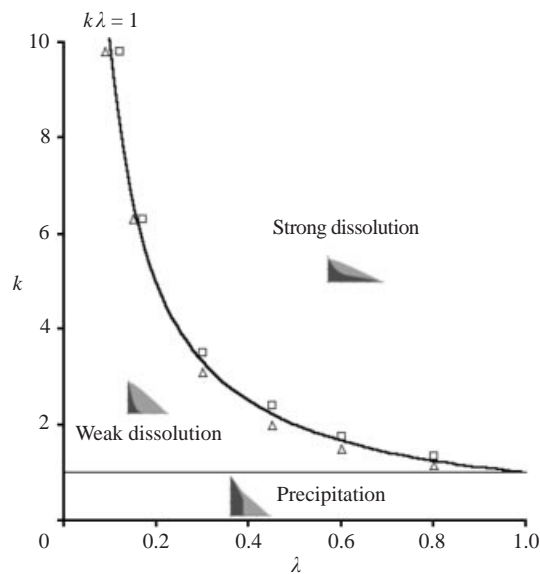

FIGURE 5. Regime diagram illustrating how the different regimes of precipitation, strong dissolution and weak dissolution reactions vary with the chemical reaction constant λ and the permeability ratio k. The curve $k\lambda = 1$ arises from the asymptotic analysis of the nose of the current.

The difference between strong and weak dissolution reactions may have important implications when monitoring the flow of tracer injected with the liquid since the fluid may advance further than the reaction zone itself.

3.4. *Precipitation solutions, $k < 1$*

The case $k < 1$ corresponds to a precipitation reaction in which the permeability increases across the the reaction front. In this case, we expect that the reaction front

will remain close to the injection site, while the reacted fluid can run far ahead of the reaction front as it moves into the original, high permeability rock. According to the equations, the gradient of the depth of the reaction front, $df_l/d\eta$, decreases until it reaches a point at which it becomes singular. Physically, this singularity arises because the reacted fluid can migrate through the high-permeability unreacted rock more rapidly than it is supplied from the low-permeability reacted rock. The location of the discontinuity, $\eta = \eta_s$, may be determined by using the reaction law (§2) which relates the flux of unreacted fluid supplied to the shock, u, say, with the speed of the shock dx/dt according to the relation

$$\frac{dx}{dt} = \lambda u.$$
(26)

This may be expressed in dimensionless terms using equations (16) and (17) as

$$\frac{df_u}{d\eta} = \frac{-2\eta_s}{3k\lambda},$$
(27)

where η_s is the location of the shock.

At the shock, $df_u/d\eta$ is not continuous. In order to conserve flux, we apply the jump condition (23) relating the flux upstream and downstream of the shock. Using these conditions, we have found a family of solutions which identify how the structure of the solution changes with λ and k (figure 6). For small λ, a very large volume of fluid is required to react with a given volume of rock, and so the reaction front remains close to the source (figure 6a). As λ increases, less fluid is required to react with a given volume of rock, and so the reacted region extends further into the current (figure 6b). For very large λ, only a small amount of liquid is required to react with a given volume of liquid, and so the reaction front extends nearly as far as the leading edge of injected fluid. As a result, the shock at the leading edge of the reaction zone becomes very small (figure 6c). As the permeability ratio associated with the precipitation increases, the rock near the source becomes progressively more clogged with precipitate. As a result, the lateral extent of the precipitation zone decreases and it deepens, with the reacted fluid running far ahead of the reaction zone (figure 6d).

3.5. *Lateral extent of the reaction zone within the injected liquid*

One of the interesting features of these similarity solutions is that the leading edge of the reaction front, η_f, may lag behind the nose of the current, η_e. In figure 7, we present a series of numerical calculations which illustrate how the ratio $N = \eta_f/\eta_e$ varies with the two control parameters, the permeability ratio k and the reaction constant λ. The calculations show that for both dissolution (solid lines) and precipitation (dashed lines) reactions, N increases with λ. Essentially, as progressively less fluid is required to react with a given volume of rock, the mass of reacted fluid occupies a progressively smaller part of the region occupied by injected fluid. The calculation also illustrates that for precipitation reactions, the reaction front only extends to the nose of the current in the limiting situation that $\lambda = 1$. This limit corresponds to the case in which the fluid effectively has an inexhaustible supply of reactant. Otherwise, there is a region at the nose of the current, ahead of the reaction zone, in which the rock is flooded with reacted source fluid. In contrast, as described in §3.2, for dissolution reactions, the reaction front reaches the nose of the current when $k\lambda \geqslant 1$.
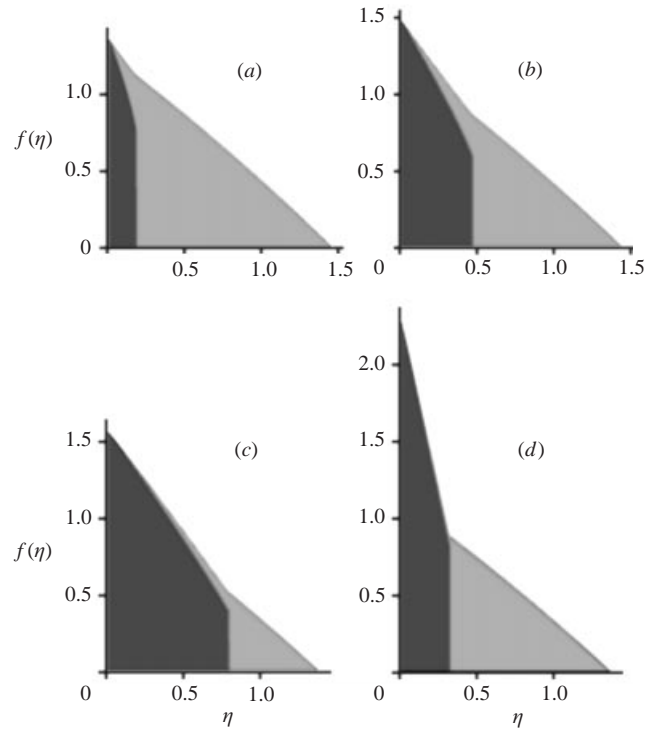
FIGURE 6. Calculations showing the shape of the reaction front and the distribution of the injected liquid in the case of a precipitation reaction. Calculations are shown for permeability ratios $k = 0.5$ with (a) $\lambda = 0.2$, (b) 0.5, (c) 0.8, and for (d) $k = 0.1$ with $\lambda = 0.5$.

4. Reactions involving a decrease in the fluid density, $R > 1$

We now extend the analysis to account for a change in density of the fluid as it passes through the reaction front. This corresponds to the case in which the reacting mineral dissolved in the liquid also contributes substantially to the density difference between the injected and formation fluids. We focus on the case in which the reaction leads to a decrease in the buoyancy of the fluid, so that the density of the reacted fluid ahead of the reaction front lies between that of the relatively high-density unreacted source fluid and the relatively low-density original formation fluid. In this case, the advancing flow is gravitationally stable and, again, we expect self-similar solutions to develop. Using the full governing equations of §2, we again seek similarity solutions for a constant injection rate Q. Now, the shape functions f_u and f_l satisfy the relations:

$$f_l - 2\eta \frac{\mathrm{d}f_l}{\mathrm{d}\eta} = 3\lambda k \frac{\mathrm{d}}{\mathrm{d}\eta} \left(f_l \left(\frac{\mathrm{d}f_u}{\mathrm{d}\eta} + (R-1)\frac{\mathrm{d}f_l}{\mathrm{d}\eta} \right) \right), \tag{28}$$

and

$$f_u - 2\eta \frac{\mathrm{d}f_u}{\mathrm{d}\eta} = 3\frac{\mathrm{d}}{\mathrm{d}\eta} \left((f_u + (k-1)f_l)\frac{\mathrm{d}f_u}{\mathrm{d}\eta} + k(R-1)f_l\frac{\mathrm{d}f_l}{\mathrm{d}\eta} \right), \tag{29}$$

and the integral conditions for the global conservation of mass and reactant, eqns (20, 21)

$$\int_0^{\eta_e} f_u \, \mathrm{d}\eta = \frac{1}{\phi}, \quad \int_0^{\eta_e} f_u \, \mathrm{d}\eta = \frac{\lambda}{\phi}. \tag{30}$$
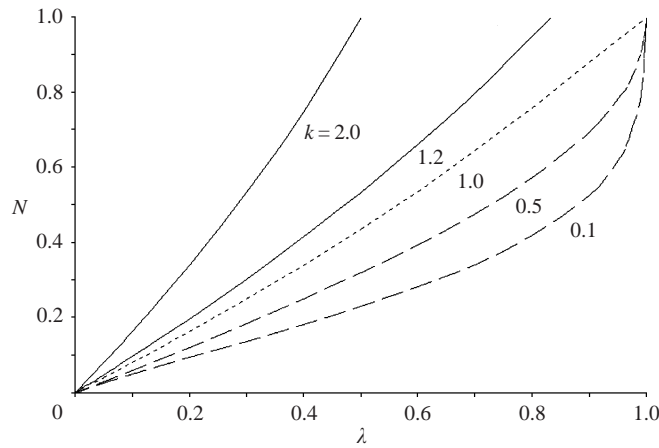
FIGURE 7. Graph showing the variation with λ of the position of the leading edge of the reaction zone as a fraction of the extent of the whole current. Calculations are shown for permeability ratios $k = 0.1, 0.5, 1.0, 1.2, 2.0$. Solid lines represent dissolution reactions while the dashed lines show precipitation. No density change, $R = 1$.

4.1. *Boundary conditions*

The additional diffusive terms in the governing equations associated with the different densities of the reacted and unreacted fluid lead to some important structural changes in the form of the solution. Most significantly, the equations are now second order in both f_u and f_l and so the shock-type solutions we found for the precipitation reactions are now smoothed out, and the depth of the reaction front decreases continuously.

Furthermore, owing to the additional flow associated with the density jump across the reaction, the depth of the layer of reacted fluid need no longer be zero at the source. This may be seen by noting that the dimensionless flux in the upper layer of reacted fluid, q_u, takes the form

$$q_u = -(f_u - f_l)\phi k \frac{\mathrm{d}f_u}{\mathrm{d}\eta}. \tag{31}$$

Since all the fluid flux at the source is unreacted fluid, it follows that $q_u = 0$ and so, from equation (31),

$$\text{either} \quad f_u = f_l \quad \text{or} \quad \frac{\mathrm{d}f_u}{\mathrm{d}\eta} = 0. \tag{32}$$

Since the dimensionless flux in the lower layer $q_l = 1$ at the source, then using (31) the two different sets of boundary conditions at $\eta = 0$ may be expressed as

$$-\phi k f_l \left(\frac{\mathrm{d}f_u}{\mathrm{d}\eta} + (R-1)\frac{\mathrm{d}f_l}{\mathrm{d}\eta} \right) = 1 \quad \text{with} \quad f_u = f_l, \tag{33}$$

or

$$-\phi k f_l(R-1)\frac{\mathrm{d}f_l}{\mathrm{d}\eta} = 1 \quad \text{with} \quad \frac{\mathrm{d}f_u}{\mathrm{d}\eta} = 0, \quad f_u \neq f_l, \tag{34}$$

In the following sections, we illustrate how there is a continuous transition from one of these regimes to the other as various parameters change. By combining these boundary conditions with the nonlinear coupled equations, we have determined the effect of gravity on the shape of the evolving reaction fronts, and we present these results in the following sections.
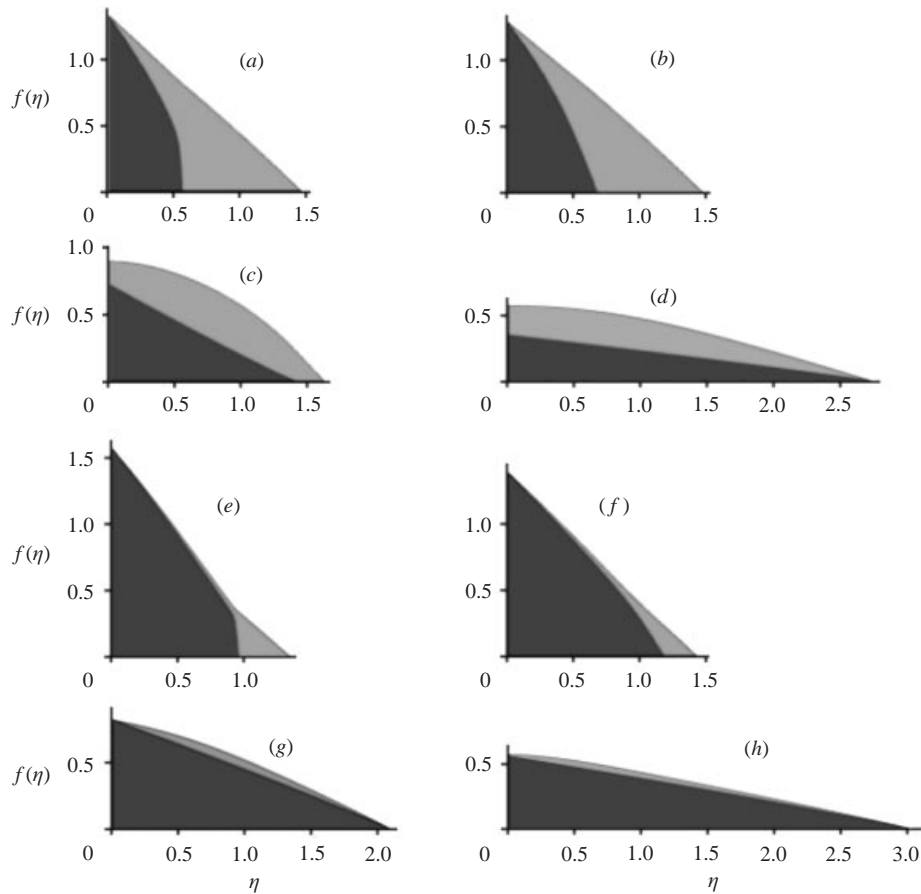
FIGURE 8. Structure of the reaction front and the injected liquid in the case where the fluid density decreases across the reaction front. Calculations are shown for precipitation reactions with parameter values (*a*)–(*d*) $k = 0.8$, $\lambda = 0.5$ with (*a*) $R = 1.005$, (*b*) 1.1, (*c*) 4.0, (*d*) 31.0, and for (*e*)–(*h*) $k = 0.5$, $\lambda = 0.9$ with (*e*) $R = 1.05$, (*f*) 1.5, (*g*) 7.0, (*h*) 21.0.

4.2. *Precipitation reactions*

We first examine the role of a density change in modifying the structure of precipitation reactions. The main consequence of a density change across the front is that the depth of the reaction zone varies continuously, and the shock-like solutions described in §3 are smoothed. For small density changes, the shocks only spread locally (figure 8*a,e*), and the solutions are similar to those presented in §3. However, as the density ratio is increased, the gravity driven slumping of the unreacted fluid begins to change the structure of the flow and the lateral extent of the reaction zone increases substantially (figure 8*b,f*). Eventually, for sufficiently large values of R, the decrease in buoyancy across the reaction front causes the injected fluid to slump under the reacted fluid, and so the depth of the reacted fluid above the source increases (figure 8*c*). The critical value at which a layer of reacted fluid begins to accumulate above the source, as a function of R and λ, is shown with the dashed line in figure 9. As λ increases, the mass of reacted fluid above the reaction front decreases, and so reacted fluid is only able to accumulate above the source if the decrease in buoyancy across the front increases.
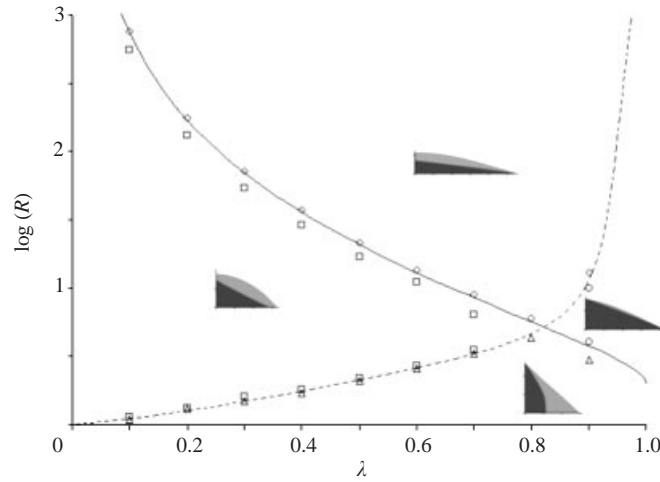
FIGURE 9. Regime diagram illustrating the different morphology of precipitation reactions, which depend on whether the reaction front extends the full length of the current and whether there is a finite depth of reacted fluid above the source. Calculations show the variation with the density ratio R and λ and are shown for one value of the permeability ratio, $k = 0.5$. ——, the predicted transition at which the leading edge of the reaction front just reaches the leading edge of the current. ----, the critical point at which a finite layer of reacted fluid accumulates above the source.

For sufficiently large R, the reaction front also spreads right to the nose of the current. All the reacted fluid then lies above the reaction zone (figure 8*d*) with the majority of the reacted fluid located near the source (figure 8*h*). The critical value of R at which the reaction front reaches the nose of the current may be found by a similar asymptotic analysis of the structure of the nose to that presented in §3.3. If the leading edge of the reaction zone coincides with the leading edge of the current, then near the nose, the coupled equations have asymptotic solution

$$f_u \sim \frac{2\eta_e}{3k\lambda(1 + \alpha(R - 1))}(\eta_e - \eta) \quad \text{for} \quad \eta < \eta_e, \quad \eta_e - \eta \ll \eta_e, \tag{35}$$

$$f_l \sim \alpha\frac{2\eta_e}{3k\lambda(1 + \alpha(R - 1))}(\eta_e - \eta) \quad \text{for} \quad \eta < \eta_e, \quad \eta_e - \eta \ll \eta_e, \tag{36}$$

with

$$\alpha = \frac{1 + k(R - 1)\lambda - k + \sqrt{(k - 1 - k(R - 1)\lambda)^2 - 4k(R - 1)(1 - \lambda k)}}{2k(R - 1)}. \tag{37}$$

In order for this solution to be possible, $f_u > 0$ and $f_l > 0$, we require that

$$\lambda \geqslant \frac{-(k + 1) + 2\sqrt{kR}}{k(R - 1)}. \tag{38}$$

Condition (38) is shown with a solid line in figure 9, and is seen to be in very good accord with our numerical calculations of the transition at which the reaction front just reaches the nose of the current.

4.3. *Dissolution reactions*

In dissolution reactions, the decrease in fluid density across the reaction front causes an increase in the lateral extent of the high-permeability zone at the base of the
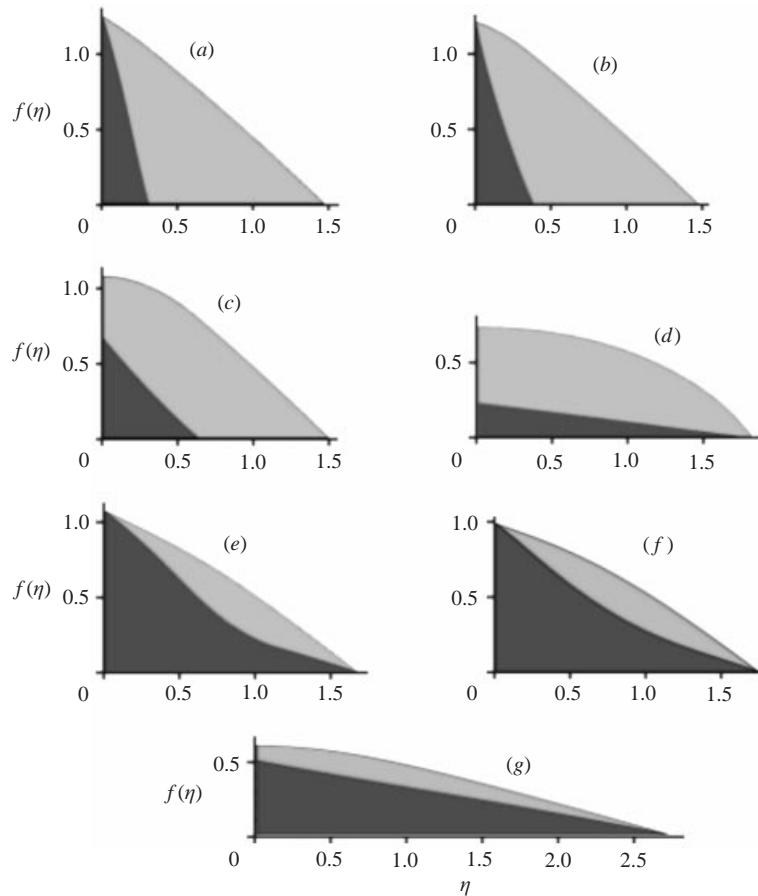
FIGURE 10. Structure of the reaction front and the injected liquid in the case where the fluid density decreases across the reaction front. Calculations are shown for dissolution reactions with parameter values (a)–(d) $k = 1.2$, $\lambda = 0.5$ with (a) $R = 1.01$, (b) 1.1, (c) 2.0, (d) 31.0, and for (e)–(g) $k = 2.0$, $\lambda = 0.7$ with (e) $R = 1.0$, (f) 1.2, (g) 6.0. Cases (a)–(c) correspond to weak dissolution reactions, whereas cases (d)–(f) correspond to strong dissolution reactions.

reservoir (figure 10a, b). Now, as in §4.2, the criterion as to whether the reaction front extends to the nose of the current is given from the asymptotic behaviour of the currents at the nose of the current. This solution has exactly the same form as (35)–(37) with the critical condition at which the reaction front just reaches the nose of the current being given by the equality in equation (38). Again, this prediction, shown as the solid line in figure 11, is in very good accord with our full numerical calculations of the location of the transition. Note also that the effect of a density change across the dissolution reaction now causes the upper layer to develop a non-zero depth (figure 10c, d, f) at $\eta = 0$ as λR increases beyond a particular value, which depends on k, shown as a dashed line in figure 11.

4.4. *Parametric study of the extent of reaction zone as a fraction of the current length*

As in §3, it is of interest to explore the extent of the reaction zone as a fraction of the total current. The general trend for both dissolution and precipitation reactions is similar, as shown in figure 12, in which we present calculations of the variation of the ratio $N = \eta_f/\eta_e$ with R and λ for a given k. The calculations show that for both
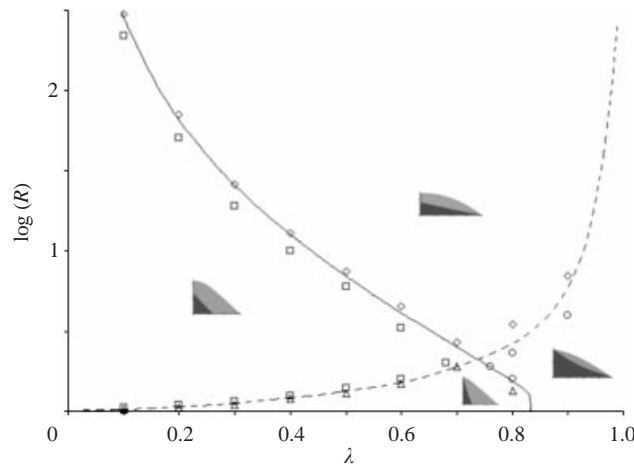
FIGURE 11. Regime diagram illustrating the different regimes of dissolution reactions, which depend on whether the reaction front extends the full length of the current and whether there is a finite depth of reacted fluid above the source. Calculations show the variation with the density ratio R and λ and are shown for one value of permeability ratio $k = 1.2$. ——, the predicted transition at which the leading edge of the reaction front just reaches the leading edge of the current. - - - -, the critical point at which a finite layer of reacted fluid accumulates above the source.
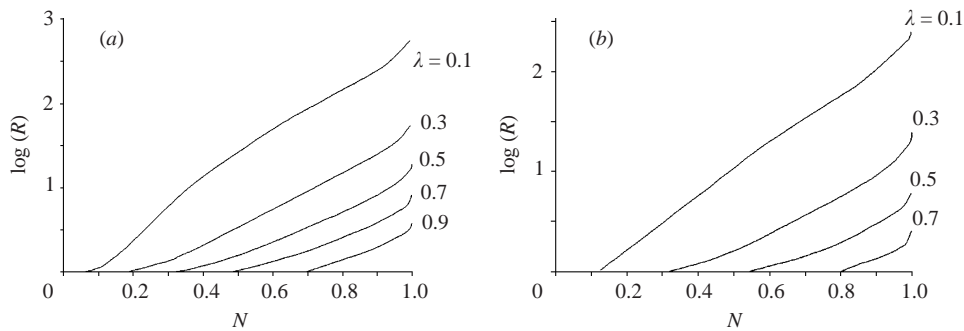

FIGURE 12. Graphs showing the effect of the density ratio R on the maximum lateral extension of the reaction zone as a fraction of the total length of the current. (*a*) Precipitation reactions are shown for $k = 0.5$ and $\lambda = 0.1, 0.3, 0.5, 0.7, 0.9$. (*b*) Dissolution reactions are shown for $k = 1.2$ and $\lambda = 0.1, 0.3, 0.5, 0.7$.

dissolution reactions (figure 12*a*) and precipitation reactions (figure 12*b*), the ratio N increases with R. As the reacted fluid becomes progressively lighter, the relatively dense unreacted fluid runs out under the less dense reacted fluid. As illustrated in §4.2, these calculations show that, with a density jump across the reaction front, precipitation reactions can now extend to the nose of the current if the buoyancy decrease across the reaction is sufficiently large.

5. Applications

Although the theoretical model presented in this work represents a considerable simplification of reaction fronts migrating through real permeable media, it is instructive to explore the implications of the model for both natural and engineered flows which drive reactions in permeable rock. According to our model, the length of the current $x \sim \gamma(\omega t)^{2/3}$ while the height of the current, $h \sim \gamma(\omega t)^{1/3}$, and so after a time

of order $1/\omega$, the reaction zone begins to become controlled by gravity, with $x > h$, and subsequently spreads according to our model.

In a natural context, the formation fluid in a permeable reservoir may be displaced by fluid of different composition owing to fracture formation connecting the reservoir to another higher-pressure permeable layer (Phillips 1991), or perhaps owing to sea-level change. Such flushing events may be responsible for the creation of so-called secondary porosity, often present in hydrocarbon reservoirs as a result of the dissolution of minerals subsequent to the geological emplacement of the reservoir. The time scale of the flows produced by such processes may be of order 10–10^4 years. In laterally extensive permeable strata, with permeability $10^{-13} \, \text{m}^2$, and with density contrasts of order $100 \, \text{kg m}^{-3}$, the typical values for the gravitational flow speed $S \sim 10^{-7} \, \text{m s}^{-1}$. The typical flow speed driven from a neighbouring high-pressure aquifer depends on the resistance to flow in any fractures connecting the two layers, but flow rates Q of order $10^{-6} \, \text{m}^2 \, \text{s}^{-1}$ might be plausible for a flow driven by a pressure difference of 10^6 Pa, over a distance $100 \, \text{m}$ along a fracture of permeability $10^{-11} \, \text{m}^2$ and width $10^{-3} \, \text{m}$. With these values of Q and S, we find ω might be of order $\omega = 10^{-8}$ while γ might be of order 10. We deduce that the flow will spread into the layer and become controlled by gravitational forces after a time of order 10 years. On time scales comparable to or longer than this, the assumption of chemical equilibrium should be appropriate, as used in the model presented above. In the case of dense input fluid, the dissolution front would then spread as a narrow reaction layer along the base of the layer, extending to a distance of order $1000 \, \text{m}$ while only deepening to depths of order 10–$100 \, \text{m}$ over the subsequent 1000 years. Indeed, if the permeability contrast associated with the dissolution reaction is sufficient, then the shape of the current will in fact increase the horizontal extent of the current by up to a factor of 10, as shown in the calculations of §§ 3 and 4. As a result, we might expect reaction zones to be horizontally extensive, and confined vertically above impermeable horizons in the formation.

In many commercially developed oil reservoirs, water is injected in order to displace the oil and increase recovery. However, in many oil reservoirs, the pore spaces also include some formation or connate water, and this too may be displaced by the injected fluid. Somewhat analogously, in geothermal reservoirs, cold water is injected into the reservoir to displace the hot fluids drawn from the system, and thereby maintain the heat exchange from the hot rock. In both systems, the injected fluid typically has a different concentration from the formation water and this may induce reactions with the porous matrix. Let us consider injection into a typical reservoir of good permeability $\sim 10^{-12} \, \text{m}^2$, porosity 0.1, with a buoyancy contrast $\Delta \rho_l / \rho \sim 0.1$, so that the typical buoyancy driven flow speed $S \sim 10^{-6} \, \text{m s}^{-1}$. For injection from a horizontal well into a confined reservoir, the flow rate may be of order $Q \sim 10^{-5} \, \text{m}^2 \, \text{s}^{-1}$ per unit length of the well. We thus find that $\gamma = 10 \, \text{m}$, and $\omega = 10^{-7} \, \text{s}^{-1}$, and so the gravity-driven flow model becomes appropriate after about 10^7–10^8 s. Subsequently, a laterally extensive gravity controlled reaction zone as described herein would be expected to develop. This time scale may be comparable to the life of a particular injection scheme, and so the model results may be useful in providing guidance on the general morphology of any reaction zones produced by the injection process, although, at earlier times the flow will be dominated by the pressure applied at the injection well.

6. Conclusions and discussion

We have developed a simplified quantitative model to describe the gravity-driven flow of reaction fronts along the base of a homogeneous porous layer. Using the

model, we have developed a series of similarity solutions which describe the evolution of both dissolution and precipitation fronts. We have found that for dissolution reactions, in which the permeability increases across the reaction, the reaction front has an elongate finger-like shape along the base of the layer. In this regime, after passing through the reaction front, the reacted fluid tends to accumulate in the lower-permeability rock above the reaction front, while the reaction zone outruns the reacted fluid along the base of the formation. In contrast, for a precipitation reaction, the reaction front tends to remain close to the source of reacting liquid and has a near vertical front at its leading edge. The reacted fluid then spreads ahead of the reaction front into the higher-permeability rock. We have shown that if the fluid undergoes a decrease in buoyancy associated with the reaction, then the reaction front tends to spread more rapidly along the base of the formation, smoothing out the discontinuity in the case of the precipitation reaction. We apply the model to the natural flooding of an aquifer or reservoir with fluid of different composition following the opening of a fracture from a higher-pressure source. We show that on time scales of 10–1000 years, the model is able to describe the leading-order structure of the reaction zone. For dissolution reactions, we predict that laterally extensive thin bands of high permeability will develop adjacent to the impermeable boundaries of a reservoir containing laterally extensive layers of high permeability.

There are several avenues for developing this work. For example, we plan to extend the modelling approach to describe the dynamics of gravity-driven reaction fronts in vertically layered reservoirs. In this situation, the reacting fluid may deepen beyond the vertical distance between adjacent low-permeability horizons. It may also drain through the low-permeability layers (cf. Pritchard, Woods & Hogg 2001). We also plan to model the dynamics of reaction fronts in which the buoyancy of the reacted fluid changes sign with respect to the formation fluid, as may occur if the solubility of the injected fluid with respect to a particular mineral exceeds that of the formation fluid.

REFERENCES

CHADAM, J., HOFF, D., MERINO, E., ORTOLEVA, P. & SEN A. 1986 Reactive-infiltration instabilities. *IMA J. Appl. Math.* **36**, 207–221.

DULLIEN, F. A. L. 1992 *Porous Media: Fluid Transport and Pore Structure.* Academic.

HINCH, E. J. & BHATT, B. S. 1990 Stability of an acid front moving through porous rock. *J. Fluid Mech.* **212**, 279–288.

HUPPERT, H. E. & WOODS, A. W. 1995 Gravity driven flows in porous layers. *J. Fluid Mech.* **292**, 55–69.

KELEMEN, P. B., WHITEHEAD, J. A., AHARONOV, E. & JORDAHL, K. A. 1995 Experiments on flow focusing in soluble porous media, with applications to melt extraction from the mantle. *J. Geophys. Res.* **100**, 475–496.

ORMOND, A. & ORTOLEVA, P. 2000 Numerical modelling of reaction-induced cavities in a porous rock. *J. Geophys. Res.* 16 737–16 747.

ORTOLEVA, P., MERINO, E., MOORE, C. & CHADAM, J. 1987 Geochemical self-organisation, I: reaction-transport feedbacks. *Am. J. Sci.* **287**, 979–1007.

PHILLIPS, O. M. 1991 *Flow and Reactions in Porous Rocks.* Cambridge University Press.

PRITCHARD, D., WOODS, A. W. & HOGG, A. J. 2001 On the slow draining of a gravity current moving through a layered permeable medium. *J. Fluid Mech.* **444**, 23–47.

WOODS, A. W. & MASON, R. 2000 The dynamics of two-layer gravity-driven flows in permeable rock. *J. Fluid Mech.* **421**, 83–114.